Available online at www.sciencedirect.com

ScienceDirect

journal homepage: www.elsevier.com/locate/he

Performance investigation of a multi-stage sorption hydrogen compressor

Sanjay Gupta, Vinod Kumar Sharma *

Department of Thermal and Energy Engineering, School of Mechanical Engineering, Vellore Institute of Technology, Vellore, 632014, India

HIGHLIGHTS

- Novel multi-stage sorption hydrogen compressor is proposed and analysed using FVM approach.
- $La_{0.9}C_{0.1}Ni_5$, $Ti_{0.98}Zr_{0.02}V_{0.43}Fe_{0.09}Cr_{0.05}Mn_{1.5}$, $MmNi_5$ and TiCrMn alloys are used as working materials.
- The maximum compression ratio of 73 with a maximum discharge of 695 bar is achieved.
- Maximum compression work of 47.34 kJ and total heat supply of 356 kJ with an overall efficiency of 13.3% is achieved.

GRAPHICAL ABSTRACT

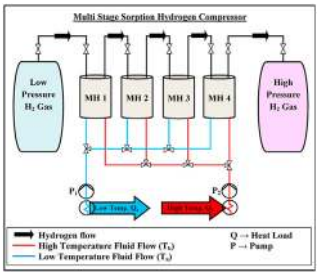

ARTICLE INFO

Article history:
Received 17 August 2020
Received in revised form
22 September 2020
Accepted 28 September 2020
Available online 23 October 2020

Keywords:
Sorption hydrogen compressor
Metal hydrides
CFD simulation
Thermodynamic cycle
Compressor work
Efficiency

ABSTRACT

Among several thermodynamic applications of metal hydrides, sorption hydrogen compressor (SHC) is more attractive for real-time application due to ease of construction and operation. In the present study, a four-stage sorption hydrogen compressor is proposed with detailed working principle for the compression output of >500 bar pressure. By adopting the screening methodology, four metal hydrides, i.e. $La_{0.9}Ce_{0.1}Ni_5$, $Ti_{0.99}Zr_{0.01}V_{0.43}Fe_{0.99}Cr_{0.05}Mn_{1.5}$, $MmNi_5$ and TiCrMn are selected for stages – 1, 2, 3 and 4 respectively with the supply temperature of 298 K and discharge temperatures of 373 K. The performance of sorption hydrogen compressor is estimated through finite volume approach and thermodynamic simulation in terms of variations in metal hydride bed pressure, temperature, hydrogen transmission, compressor work and efficiency. The numerical model is validated with experimentally measured metal hydride bed temperature and hydrogen concentration for single-stage hydrogen compressor, which are observed to be in good agreement. The cycle time of multi-stage SHC is predicted to be ~100 min with the maximum compression ratio of 73 with an overall efficiency of 10.62% employing 0.5 kg of each alloy and supply pressure of 9.5 bar. It is also observed that the discharge temperature greatly influences system performance. The dynamic performance of the system is also estimated with the implementation of simulation generated property data and observed

* *Corresponding author.*
E-mail address: vinsharma85@gmail.com (V.K. Sharma).
https://doi.org/10.1016/j.ijhydene.2020.09.249

that the performance parameters increased with the progression of hydrogen transmission.

Introduction

In sorption hydrogen compressor, the heat interactions during hydrogen absorption and desorption in metal hydrides are employed to run the system as well as the phenomena of increase in plateau pressure by heating is used for hydrogen compression. The main advantages of metal hydride based sorption hydrogen compressor are: ease of design and development (i.e. compact and safe), the nonexistence of mechanical moving parts, reliable and can be operated using waste heat. Very high-pressure hydrogen is used in hydrogen-fuelled vehicles and other industrial applications. Hydrogen compression system, in refuelling stations, is highly responsible for higher infrastructure and operation cost. Sorption hydrogen compressor can help to reduce this cost due to the advantages mentioned above.

Metal hydrides are used worldwide in several research institutes, nuclear and defence industries for many years to store and process hydrogen isotopes, protium, deuterium and tritium [1,2]. The first prototype of metal hydride based water pump was tested in Sandia National Laboratories with the working temperature range of 20–80 °C [3]. The performance measurement of energy conversion system with the application of coupled sorption hydrogen compressor and conventional organic Rankine cycle concluded that the compression of hydrogen through sorption system is much efficient because of low operating cost, high COP and power output [4].

A research team of Srinivasa Murthy at IIT Madras [5–7] have measured the performance of SHC theoretically and experimentally. In 2002 [7], a parametric study on single-stage SHC is carried out and reported the hydrogen delivery pressure of 64 bar at 340 K with a supply pressure of 8 bar using $Ti_{0.98}Zr_{0.02}V_{0.43}Fe_{0.09}Cr_{0.05}Mn_{1.5}$. Later, another single-stage SHC is tested by employing $MnNi_{4.6}Al_{0.4}$ alloy and reported the system efficiency of 7.3% and a pressure ratio of 8.8 at 90 °C. Later in 2012 [8], a research team of Muthukumar at IIT Guwahati have conducted a numerical investigation on three-stage SHC. The series of alloys used are $LaNi_5$, $MmNi_{4.6}Al_{0.4}$ and $Ti_{0.98}Zr_{0.02}V_{0.43}Fe_{0.09}Cr_{0.05}Mn_{1.5}$. The maximum storage pressure of 100 bar is predicted at a delivery temperature of 120 °C for the supply pressure of 2.5 bar at 20 °C. Later, Anil Kumar and the team at IIT Indore [9] have developed and tested a single-stage SHC using $La_{0.8}Ce_{0.2}Ni_5$ alloys in three different bed patterns, i.e. lose metal hydride powder, pallets of MH mixed with graphite flakes and pallets of MH mixed with graphite flakes and embedded with copper wire mesh. Hydrogen compression was reported as 35 bar at 80 °C from 10 bar at 20 °C. Recently, a thermodynamic simulation of double-stage SHC is reported by Vinod and Anil [10] using $La_{0.9}Ce_{0.1}Ni_5$ and $La_{0.8}Ce_{0.2}Ni_5$ in series. It is reported that hydrogen can be compressed from 4.5 bar at 20 °C to 75 bar at 80 °C with a cycle efficiency of 12.5%. Karagiorgis et al. [11] developed a novel six-stage SHC operates between 10 and 80 °C. Hydrogen compression takes place up to 22 MPa from 0.7 MPa supply pressure. In each MH compression stages, 6.2 kg of material was used. The detail observations on studies carried out by several researchers on the development of sorption hydrogen compressors are presented in Table 1.

It is observed from the detailed literature review on metal hydride based SHC that several experimental and theoretical studies were carried out on the development of single and multi-stage sorption hydrogen compressors. But, the thermal compressor for hydrogen delivery at a pressure of more than 500 bar is not tested yet either experimentally or numerically. In continuation with that, in the present study, a four-stage SHC is proposed to achieve the hydrogen compression more than 500 bar pressure. It is also observed that minimal studies were carried out on a screening of working pairs and performance prediction of SHC. Apart from that, the effect of hydrogen transmission rate and amount on system performance is never being attempted. Therefore, in the present study, a novel four-stage metal hydride based sorption hydrogen compressor is proposed and evaluated its performance for the delivery pressure of 695 bar at 373 K with the initial supply pressure of 9.5 bar at 298 K. The detailed methodology on screening of working pair and performance prediction are also presented. Based on the previous studies and screening methodology; a set of $La_{0.9}Ce_{0.1}Ni_5$, $Ti_{0.99}Zr_{0.01}V_{0.43}Fe_{0.99}Cr_{0.05}Mn_{1.5}$, $MmNi_5$ and TiCrMn alloys are chosen in each stage of hydrogen compression. The performance of four-stage SHC in terms of metal hydride bed pressure, temperature, hydrogen concentration, compression work and efficiency is evaluated through thermodynamic and heat – mass transfer (Finite Volume Approach) analyses. Besides, the thermodynamic performance of SHC is evaluated for static as well as dynamic conditions by employing the numerically predicted hydrogen transfer behaviour (rate and amount). Lastly, the performance of the system is also estimated for a large mass of metal hydrides (i.e. 10 kg of each MH) to predict its performance for massive output. The study is further extended to determine the influence of discharge temperature on system performance.

Working principle of multi-stage sorption hydrogen compressor

Before understanding the working principle of sorption hydrogen compressor, a little information about metal hydride formation and decomposition is vital to keep in mind. It is well known that the metal hydrides are formed by the interaction of special alloys with hydrogen with the release of

Table 1 – Summary of literature on single and multi-stage sorption hydrogen compressor.

S. No.	Study	Material used	Observations/Remarks	Reference
1	A numerical study was carried out on single-stage sorption hydrogen compressor for the production of 48 bar hydrogen at 465 K.	$La_{0.1}Ni_{4.78}Sn_{0.22}$	It is reported that for the production of 48 bar at 465 K, the absorption pressure of the hydride should be less than 0.3 bar at 282 K. The plateau slope must be relatively flat at low as well as high temperature to reduce the power input. The plateau slope increases with the number of cycles due to degradation of hydride powder.	[12]
2	Experimental studies were carried out on single and double stage hydrogen compressors for the high-pressure hydrogen output of 45 MPa at 170 °C from 4 MPa at 20 °C.	$(MmLaCa)(NiAl)_5$ and $Ti_{1+x}(CrMnV)_2$	Properties of different AB5 and AB2 type metal hydride were studied to determine their suitability for hydrogen compressor. For the development of single-stage compressor, $MmNi_5$ was selected, but due to the high hysteresis and poor activation properties La, Al and Ca are added, and finally, $Mm_{0.7}Ca_{0.2}La_{0.1}(Ni_{4.95}Al_{0.05})$ was chosen. The hydrogen compression rate of 40 L/min was reported. Similarly, $Ti_{1+x}Cr_{2-y}$(Mn,V)y (x = 0.0.2; y = 0.4.0.8) were selected for the double stage hydrogen compressor, and the compression rate was observed to be 20 L/min. The heat transfer medium used in the single-stage was oil, whereas it is water in case of the dual-stage.	[13]
3	Experimental study on two-stage hydrogen compressor with the employment of AB5 and AB2 type metal hydrides for the production of 74.5 MPa hydrogen was carried out.	$La_{0.35}Ce_{0.45}Ca_{0.2}Ni_{4.95}Al_{0.05}$ alloy and $Ti_{0.8}Zr_{0.2}Cr_{0.95}Fe_{0.95}V_{0.1}$	$La_{0.35}Ce_{0.45}Ca_{0.2}Ni_{4.95}Al_{0.05}$ alloy and $Ti_{0.8}Zr_{0.2}Cr_{0.95}Fe_{0.95}V_{0.1}$ alloy are developed and used as the first stage and second stage metal hydrides, respectively. A setup was built and tested with a hydrogen compression capacity of around 2000 L per cycle with oil as a heat exchange medium of 423 K maximum temperature, which produces hydrogen pressure of 74.5 MPa. The hydrogen flow rate of the compressor was 34.6 L per minute.	[14]
4	Experimental studies on the two-stage compressor for hydrogen output of 55 MPa was carried out.	$LaNi_5$ and $Ca_{0.6}Mm_{0.4}Ni_5$	The first reactor contains 5 g of $LaNi_5$ and second reactor contains 3 g of $Ca_{0.6}Mm_{0.4}Ni_5$ and Sn binder mass of 0.3 g. The thickness of the reactor tube walls was 0.12 inches to withstand maximum operating pressure up to 55 MPa. The compression ratio of 12 was achieved when the limit of the operating temperature was maintained between 10 °C and 90 °C.	[15]
5	Hydrogen compressor was developed and tested for compressing hydrogen from 0.02 MPa to 3.3 MPa.	$LaNi_{4.8}Sn_{0.2}$ and $LaNi_{4.25}Al_{0.75}$	45 kg of $LaNi_{4.8}Sn_{0.2}$ and 3.5 kg of $LaNi_{4.25}Al_{0.75}$ are used for the system. The effect of heat transfer management was studied with the implementation of fin and reported that the reactor with fins possessed high heat transfer efficiency than without fins. The performance of the compressor was tested for 207 cycles with the pressure range of 0.3–3.3 MPa at 310–450 K for $LaNi_{4.8}Sn_{0.2}$ and 0.02–0.3 MPa at 315–410 K for $LaNi_{4.25}Al_{0.75}$.	[16]
6	Experimental studies on single and dual-stage hydrogen compressor were carried out.	$LaNi_5$, $Ca_{0.6}Mm_{0.4}Ni_5$ and $Ca_{0.2}Mm_{0.8}Ni_5$	In a single-stage compressor, with the high supply pressure, $Ca_{0.2}Mm_{0.8}Ni_5$ possessed 56% and 14.7% higher compressor ratio compared to $LaNi_5$ and $Ca_{0.6}Mm_{0.4}Ni_5$, whereas at low supply pressure, it is almost same. In a dual-stage system, the pair of $LaNi_5$ - $Ca_{0.2}Mm_{0.8}Ni_5$ possesses 53% higher compression ration than that of pair $LaNi_5$ - $Ca_{0.6}Mm_{0.4}Ni_5$. It is also reported that the reactor design and screening of a working pair greatly influence system performance.	[17]
7	Experimental investigation on the three-stage hydrogen compressor was carried out.	$LaNi_{4.8}Sn_{0.2}$, $LaNi_5$ and $MmNi_{4.7}Al_{0.3}$	A part of the hydrogen produced from the electrolyser is compressed and achieved the overall compression ratio of 20:1 when it is operating between 20 °C and 80 °C.	[18,19]

8	Thermodynamic simulation of single and three-stage hydrogen compressor is carried out.	$Ti_{0.85}Zr_{0.15}Mn_{1.33}V_{0.3}$, $Ti_{0.8}Zr_{0.2}Mn_{1.2}Cr_{0.6}V_{0.2}$ and $Ti_{0.9}Zr_{0.1}Mn_{1.47}Cr_{0.4}V_{0.2}$	Two different metal samples of AB_2 type were synthesised. A low-pressure $Ti_{0.9}Zr_{0.1}Mn_{1.34}V_{0.3}$ alloy and a high-pressure $Ti_{0.9}Zr_{0.1}Mn_{1.47}Cr_{0.4}V_{0.2}$ alloy are considered. The reactor temperatures are operating between 296 K and 353 K. The work is extended to investigate the thermodynamic model of three-stage MH hydrogen compressor using AB_2 alloys, which are synthesised by arc melting process. The selected alloys were $Ti_{0.85}Zr_{0.15}Mn_{1.33}V_{0.3}$, $Ti_{0.8}Zr_{0.2}Mn_{1.2}Cr_{0.6}V_{0.2}$ and $Ti_{0.9}Zr_{0.1}Mn_{1.47}Cr_{0.4}V_{0.2}$ as low, medium and high-pressure metal hydrides respectively, which are operating between 23 and 80 °C. However, the optimum desorption temperature for three stages was identified within 110–132 °C, and the overall compression ratio was about 92. It is also concluded that the amount of compressed hydrogen, the mass of alloy and volume of reactors linearly depend on the volume of a compressed hydrogen storage tank.	[20,21]
9	Characterisation of metal hydride for hydrogen compressor application was presented.	40 Ve20Tie40Cr (at%)	A high-pressure capacity apparatus is developed for the characterisation of a metal hydride, i.e. 40 Ve20Tie40Cr (at%) in the pressure range up to 1000 bar and 200 °C temperature. The compression of hydrogen from 21 bar to 300 bar is achieved with the hydrogen concentration of 1.8 wt% at 200 °C.	[22]
10	Performance evaluation of real-time hydrogen compressor installed in the fuel station was carried out.	–	Authors have presented the successful onsite operation of SSHC equipped in hydrogen refuelling station in South Africa over three years period. This SSHC has several advantages like simplicity in design, capital cost, operational cost, safety and reliability, and noiseless operation over the conventional compressors, which are currently used. The system delivers 13 Nm3/h of hydrogen at 185 bar pressure using steam heat at 140 °C, whereas uses water at 20 °C for cooling the system. The above report proves the feasibility of sorption hydrogen compressor for high-pressure hydrogen output in real practice.	[23]
11	Experimental and numerical investigations on two-stage hydrogen compressor were carried out.	$LaNi_5$ and $La_{0.5}Ce_{0.5}Ni_5$ alloys	In the first stage, 0.85 kg of $LaNi_5$ was used, whereas 0.7 kg of $La_{0.5}Ce_{0.5}Ni_5$ was used in the second stage. The absorption was done at 20 °C, and the desorption of hydrogen occurred at 140 °C, which produces the hydrogen at a pressure more than 100 bar in 2.5 h.	[24]
12	Numerical study on three-stage hydrogen compressor was carried out using AB_5 and AB_2 type metal hydrides.	LaNi5, MmNi4. 6Al0.4 and AB2 intermetallic alloys	The working principle of the three-stage compressor and modelling scheme was presented. The results are validated with previous experimental data and observed to be in good agreement. The temperature limits are fixed between 20 and 130 °C. The compression ratio of 22:1 is obtained with the maximum pressure at the end of the last dehydrogenation process delivers 315 bar. The work was extended for seven-stage MH hydrogen compressor with relatively low-temperature ranges of 10–80 °C and achieved a compression ratio of 18.7. The total energy demand required for attaining the compression ratio of 18.7 was about 37.96 kWh. When the desorption temperature is increased to 120 °C, the compression ratio and the total energy demand were found to be increased to 41.5 and 56.05 kWh, respectively.	[25,26]

absorption heat, whereas it can be decomposed with the supply of external heat. The formation of metal hydride takes place in three phases, i.e. solid solution (α), plateau (α+β) and hydride (β). Here, plateau region is critical because it plays a vital role in the development of any MH based thermodynamic device and the storage capacity within this region is a reversible storage capacity of a metal hydride, which gets exchanged between coupled MH beds. It is also important to note that the plateau pressure increases drastically with a marginal increase in operating temperature. This pressure upsurge capacity dramatically depends on the type of metal hydrides that classifies it into low-pressure, medium-pressure and high-pressure type metal hydrides. For the application of hydrogen compressor, high-pressure metal hydrides are a better option. The above information is required because, in basic SHC, the low-pressure hydrogen is absorbed by metal hydride at lower temperature and by heating the MH bed; high-pressure hydrogen can be delivered.

Figure 1 shows the schematic of the multi-stage sorption hydrogen compressor, whereas Fig. 2 (a) and (b) show its working principle on PCIs and van't Hoff plot, and thermodynamic cycle, respectively. Four metal hydride reactors, i.e. MH 1, MH 2, MH 3 and MH 4 can be seen in Fig. 1. All the reactor are connected with low temperature and high-temperature heat sources for cooling and heating of reactors to facilitate the absorption and desorption of hydrogen, respectively. MH 1 is connected with low-pressure hydrogen supply cylinder, and MH 4 is connected with high-pressure hydrogen storage cylinder, whereas MH 1 – MH 2, MH 2 – MH 3 and MH 3 – MH 4 are interconnected for hydrogen transmission. The system also consists of pumps and valves for heat transfer fluid flow and control.

As already mentioned that the thermodynamic sorption system considered being works within plateau region of employed metal hydrides, refer to Fig. 2 (a and b), point 1 (i.e. $\alpha \rightarrow \alpha+\beta$) shows the start of absorption of hydrogen, in MH 1, supplied from supply cylinder at a saturation pressure of MH 1. With the absorption of hydrogen, the equilibrium pressure of MH 1 increases to point 1' (i.e. $\alpha+\beta \rightarrow \beta$) at a temperature T_l with the release of absorption heat (Q_a). After that, MH 1 is sensibly heated to T_h (i.e. its desorption temperature), which drastically increases its equilibrium pressure and is denoted by point 2. This is the end of the first stage; after that, the hydrogen stored in MH 1 gets desorbed with the help of desorption heat (Q_h) at T_h. This desorbed hydrogen is absorbed by MH 2, which is coupled with MH 1. Condition of MH 2 at the beginning of absorption is denoted by point 3, whereas conditions of MH 1 and MH 2, at the end of desorption and absorption processes, are denoted by point 2′ and 3′, respectively. It is to be noted that high-pressure difference is available between MH 1 (point 2) and MH 2 (point 3) to facilitate the hydrogen transmission. Stage 2 completes with the sensible heating of MH 2 from point 3′ to point 4. Similar to stage 2, in stage 3, MH 2 desorbs hydrogen which is absorbed by MH 3 at state points 4 and 5 respectively. Upon hydrogen transmission, the pressure of MH 2 decreases from 4 to 4′ and pressure of MH 3 increases from 5 to 5'. At the end of the sensible heating of MH 3 at point 5, stage 3 completes. Now, in stage - 4, hydrogen transmits from MH 3 to MH 4 and their states changes from 6 to 6′ and 7 to 7′, respectively. This is due

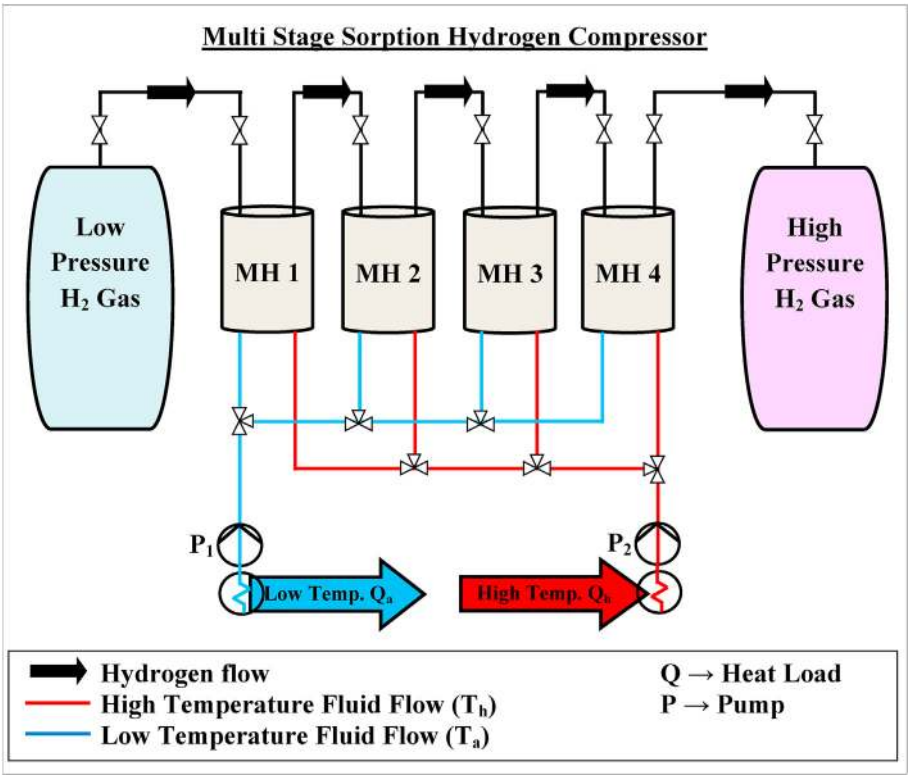

Fig. 1 – Schematic of the multi-stage sorption hydrogen compressor.

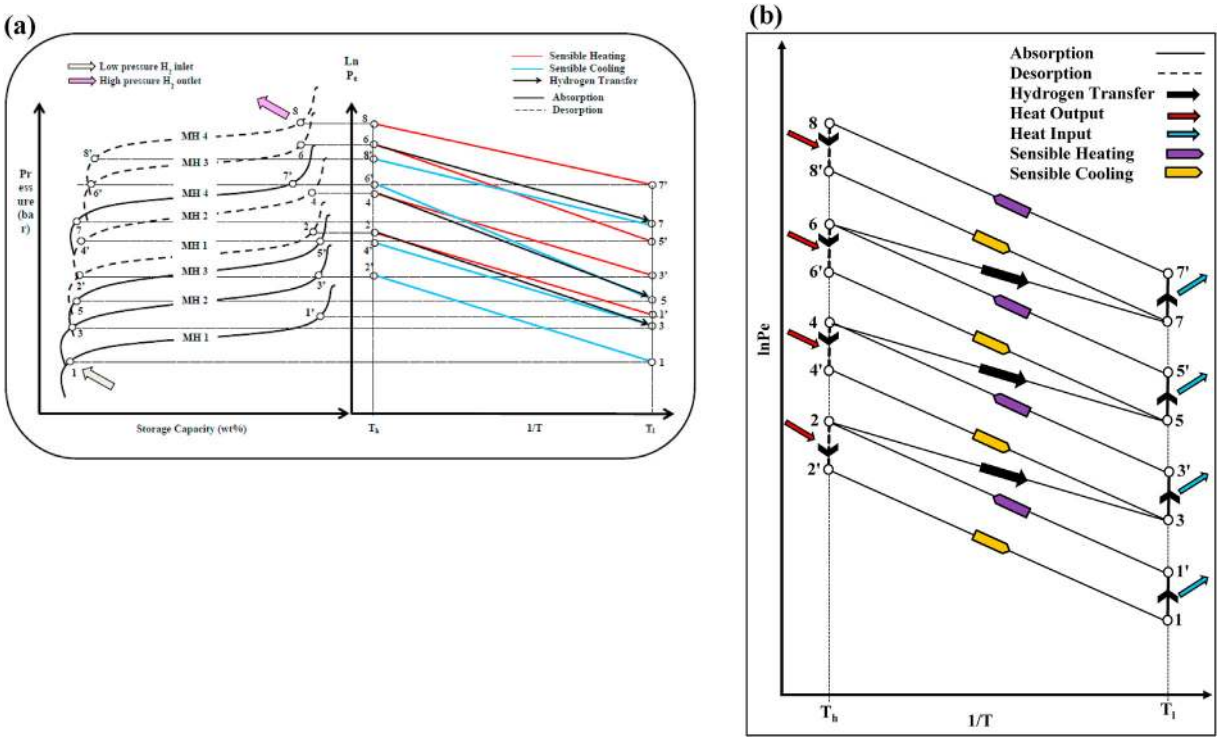

Fig. 2 – (a) PCI and van't Hoff representation of multi-stage SHC cycle. (b) Thermodynamic cycle.

to the decrease and increase in bed pressures, respectively. The reactor 4 is sensibly heated to T_h, i.e. to point 8, which is the highest pressure and discharge point of the system. At this point, the high-pressure hydrogen is delivered to the storage cylinder. The condition of MH 4 at the end of desorption is denoted by point 8'. After that, reactors are sensibly cooled to original conditions, i.e. MH 1 from 2′ to 1, MH 2 from 4′ to 3, MH 3 from 6′ to 5 and MH 4 from 8′ to 7. This process prepares the system for the next compression cycle.

It is to be noted that in all the 4 stages there exist large pressure difference between coupled reactors, i.e. processes 2 to 3, 4 to 5 and 6 to 7 to facilitate the fast and high hydrogen transmission. Also, points 2, 4, 6 and 8 are the maximum pressure states at the end of each stage. The hydrogen transmission between coupled beds stops when the pressure among both the reactors reach equilibrium. This can be seen in Fig. 2 (a) and (b) with the pressure equilibrium of reactors MH 1 (point 2′) – MH 2 (point 3′), MH 2 (point 4′) – MH 3 (point 5′) and MH 3 (point 6′) – MH 4 (point 7′). It can also be seen from Fig. 2 that at the end of sensible heating of metal hydrides its pressure increased significantly. All the absorption processes occurred at T_l with the rejection of absorption heat, whereas all desorption processes occurred at T_h with the consumption of desorption heat. The amount of absorption and desorption heats are different for different metal hydrides and depend upon their thermodynamic properties.

Screening of alloys

High reversible storage capacities, reaction enthalpies and fast kinetics involved during the formation and decomposition of metal hydrides are the main contributors in the development of any thermal device. Apart from these favourable properties, the metal hydride should possess flatter plateau, minimum hysteresis as well as higher plateau pressure at lower operating temperatures. The difference in pressure between MH beds is also one of the major factors that significantly affect the amount of hydrogen transmission from one to other. It is observed from the literature review that La based, Mm-based and Ti-based metal hydrides are widely used for the development of sorption hydrogen compressors due to their high reversible hydrogen storage capacity, high plateau pressure and thermal stability. By keeping this in mind, in the present study, screening of metal hydrides is carried out by floating various AB_5, AB and AB_2 type metal hydrides in a code generated in visual-basic for screening. The metal hydrides used for screening, along with their properties, are listed in Table 2.

A computer code for the screening of working materials is generated based on the requirements of best-suited alloys for four-stage sorption hydrogen compressor working with supply temperature of 298 K and discharge temperature of 373 K for a delivery pressure of >500 bar. The ambient temperature is chosen as supply temperature, whereas a discharge temperature of 373 K is chosen to facilitate the utilisation of solar energy or industrial waste heat as an input. It is also ensured during code generation that sufficient pressure difference must exist between coupled bed to enable the full absorption and desorption of hydrogen. In a combination of above properties, the material should possess low desorption enthalpy that can reduce the heat input to the system consequently increases efficiency. Based on the above screening procedure, out of several metal hydrides, a set of $La_{0.9}Ce_{0.1}Ni_5$,

Table 2 – List of metal hydrides used for screening of working materials.

S. No.	Materials	Enthalpy (ΔH) (kJ/molH_2)	Entropy (ΔS) (J/K molH_2)	Maximum Storage Capacity (wt%)/Temp (°C)	Reference
1	$MmNi_{4.8}Al_{0.2}$	31.16	101.2	1.28/23	[27]
2	$LaNi_{4.7}Sn_{0.3}$	36.51	112.6	1.04/24.9	[28]
3	$MmNi_{4.7}Sn_{0.3}$	31.83	106.8	0.97	[28]
4	$LmNi_{4.9}Sn_{0.1}$	28.97	104.3	1.29/23	[27]
5	$MmNi_{4.7}Al_{0.3}$	27.50	107.6	1.21/23	[27]
6	$LaNi_{4.8}Sn_{0.2}$	31.3	101	1.28/22	[19]
7	$LaNi_5$	30.7	110	1.29/21	[19]
8	$MmNi_{4.9}Fe_{0.1}$	24.8	84.7	1.2	[29]
9	$MmNi_5$	20.3	101.4	1.44/20	[30]
10	$MmNi_{4.5}Al_{0.5}$	24.41	97.04	1.36/20	[30]
11	$MmNi_4Al$	26.17	79.9	1.30/20	[30]
12	$MmNi_{3.7}Co_{0.7}Mn_{0.3}Al_{0.3}$	33.11	96.94	1.16/20	[30]
13	$MmNi_{3.5}Co_{0.4}Mn_{0.4}Al_{0.4}Fe_{0.3}$	34.27	97.82	1.05/20	[30]
14	$La_{0.8}Ce_{0.2}Ni_5$	26.6	107.3	1.4/20	[31]
15	$La_{0.9}Ce_{0.1}Ni5$	32.9	121	1.3/40	[32]
16	$LaNi_{4.6}Al_{0.4}$	34.04	108	1.41/20	[33]
17	$LaNi_{4.7}Al_{0.3}$	32.7	105	1.22	[34]
18	$MmNi_{4.2}Al_{0.8}$	25.09	120	1.3/25	[35]
19	$LaNi_{4.85}Al_{0.15}$	31.6	106	1.25	[36,37]
20	$MmNi_{4.85}Al_{0.15}$	21.05	93.9	1.4/20	[37]
21	$LaNi_{4.85}Sn_{0.15}$	29.8	105	1.3/30	[37]
22	$MmNi_{4.6}Al_{0.4}$	28	107.2	0.95/20	[38,39]
23	$MmNi_{4.6}Fe_{0.4}$	27.5	105	1.15/20	[38,40]
24	$LaNi_{4.5}Sn_{0.5}$	36	97	0.95/26.8	[41]
25	$Mm_{0.5}La_{0.5}Ni_{4.7}Sn_{0.3}$	33.8	111.2	–	[42]
26	$LaNi_{4.8}Al_{0.2}$	30.4	101.6	–	[42]
27	$MmNi_{4.7}Fe_{0.3}$	25.0	87.4	–	[42]
28	$TiFe_{0.9}Mn_{0.1}$	29.7	107.7	–	[42]
29	$La_{0.85}Ce_{0.1}5Ni_5$	24.3	91.28	–	[42]
30	$ZrFe_{1.8}Ni_{0.2}$	17.2	119.7	–	[42]
31	$Ti_{0.98}Zr_{0.02}V_{0.43}Fe_{0.09}Cr_{0.05}Mn_{1.5}$	27.4	112	1.5	[43]
32	$Zr_{0.9}Ti_{0.1}Cr_{0.9}Fe_{1.1}$	29.6	92.0	–	[44]
33	$Ti_{1.05}Fe_{0.9}Nb_{0.1}$	28.5	98.9	–	[45]
34	$Ti_{1.05}Fe_{0.8}Ni_{0.15}Cr_{0.05}$	42.5	120.6	–	[45]
35	$LaNi_{2.5}Co_{2.5}$	24.4	76.6	–	[45]
36	$LaNi_{2.5}Co_{2.4}Si_{0.1}$	27.6	81.9	–	[45]
37	TiCrMn	19.6	106	–	[46]
38	$Ti_{1.1}CrMn$	22	113.4	1.5	[47]
39	$Ti_{0.9}Zr_{0.1}Mn_{1.34}V_{0.3}$	28.7	93.5	1.65	[20]
40	$Ti_{0.5}V_{0.45}Nb_{0.05}Mn$	25.71	109.73	1.26	[48]
41	$Ti_{0.5}V_{0.4}Nb_{0.1}Mn$	23.68	104.48	1.55	[48]
42	$LaNi_{4.61}Mn_{0.26}Al_{0.13}$	36.9	109.7	–	[44]
43	$La_{0.6}Y_{0.4}Ni_{4.8}Mn_{0.2}$	26.9	102.3	–	[44]
44	$LmNi_{4.91}Sn_{0.1}$	27.2	103.1	1.3	[44]
45	$Ti_{0.99}Zr_{0.01}V_{0.43}Fe_{0.09}Cr_{0.05}Mn_{1.5}$	20	97	1.99	[44]
46	$LaNi_{4.6}Al_{0.4}$	34.8	113.9	–	[44]
47	$Zr_{0.9}Ti_{0.1}Cr_{0.6}Fe_{1.4}$	24.55	92	–	[44]
48	$LaNi_{4.35}Al_{0.65}$	34.9	104	1.13	[49]
49	$La_{0.8}Mm_{0.2}Ni_{4.9}Fe_{0.1}$	23.56	85.39	1.65	[50]
50	$La_{0.6}Mm_{0.4}Ni_{4.9}Fe_{0.1}$	22.55	89.38	1.62	[50]
51	$La_{0.4}Mm_{0.6}Ni_{4.9}Fe_{0.1}$	17.48	75.53	1.6	[50]
52	$LmNi_{4.91}Sn_{0.15}$	31	115	1.61	[51]
53	$MmNi_{4.9}Fe_{0.1}$	24.8	84.7	1.66	[29]
54	$MmNi_{4.5}Fe_{0.5}$	26	91.6	1.46	[29]
55	$MmNi_{3.4}Co_{0.5}Al_{0.3}Mn_{0.5}$	39.1	121.7	–	[45]
56	$MlNi_{3.4}Co_{0.8}Al_{0.3}Mn_{0.5}$	34.43	95.59	–	[45]
57	$Ca_{0.6}Mm_{0.4}Ni_5$	26.6	100	–	[15]
58	ZrCo	97.8	145.5	–	[52]
59	Mg_2Ni	64.5	124.5	3.52	[53]

$Ti_{0.99}Zr_{0.01}V_{0.43}Fe_{0.99}Cr_{0.05}Mn_{1.5}$, $MmNi_5$ and TiCrMn alloys is found suitable for stage 1, stage 2, stage 3 and stage 4 respectively, to produce favourable performance with high-pressure discharge. The properties of chosen metal hydrides used for present work are presented in Table 3.

Numerical modelling

The detailed methodology adopted for the present study, including geometry, governing equations, solution scheme and thermodynamic performance parameters is presented in following sub-sections.

Metal hydride reactor

The reactor geometry used in the present simulation is shown in Fig. 3. Since it is a four-stage system, a total of four reactors are required in series filled with four different metal hydrides. The dimensions of all the reactors are kept the same, i.e. 168 mm length and 33 mm diameter, to accommodate about 0.5 kg of alloy. The water jacket is also provided at an annulus for supply and extraction of heat during the reactions. A provision for hydrogen supply to MH 1 reactor and an exit from MH 4 reactor is provided. The ¼ inch tube with multiple tapered holes is provided at the centre of the cylinder to ensure the proper distribution of hydrogen gas throughout the length of the cylinder. A hydrogen supply tube with multiple holes helps to reduce reaction time. The reactors are also connected with ¼ inch tube provided with valves. Filters are provided to protect the drawing off of metal hydride particles during desorption as well as to ensure the supply of pure gas without impurities. Several thermocouples are provided at different locations to record the average bed temperature during hydrogenation and dehydrogenation.

Governing equations and boundary conditions

For the prediction of hydrogen compression performance, pressure and energy equations are discretised to transform differential equations to algebraic equations. The generated algebraic equations are solved by considering numerous boundary conditions and assumptions. During the simulation, the existence of thermal equilibrium among alloy and H_2 is assumed. The effect of heat transfer through radiation is not considered. The effect of pressure and hydrogen concentration on reaction enthalpy and entropy is negligible as well as heat transfer from the reactor to ambient is considered negligible. Following equations are used for the performance prediction of SHC concerning Fig. 2.

Hydrogen absorption in the first stage (Process 1 to 1′)
The hydrogen is supplied to the MH 1 at low pressure and temperature. The low-pressure metal hydride absorbs the hydrogen. The equilibrium pressure inside the reaction bed is calculated using the van't Hoff Equation. Assume, the initial temperature is 298 K, and the concentration of hydrogen is minimum.

$$P_{eq} = 10^5 \exp\left[\frac{\Delta H}{R_u T} - \frac{\Delta S}{R_u} + (\varphi \pm \varphi_0)\tan\left[\pi\left(\frac{x}{x_f} - \frac{1}{2}\right)\right] \pm \frac{\beta}{2}\right] \quad (1)$$

where enthalpy of formation (ΔH) and entropy formation (ΔS) are taken from previous studies, slope (φ, φ_o) and hysteresis factors (β) are calculated from PCIs. The mass of hydrogen absorbed by the metal hydride is calculated using the following equation.

$$m_{H_2} = C_a \exp\left(\frac{-E_a}{R_u T}\right) \ln\left(\frac{P_s}{P_{eq}}\right)(\rho_{ss} - \rho_s) \quad (2)$$

The increase in temperature within the reaction bed is determined by solving the following energy equation.

$$(\rho C_p)_e \frac{\partial T}{\partial t} + (\rho C_p)_g \vec{u}.\nabla T = \lambda_e \nabla^2 T + m_{H_2}\left[\frac{\Delta H}{M_g} - T(C_{P,g} - C_{P,s})\right] \quad (3)$$

The heat generated within the reactor can be effectively removed by the heat transfer fluid circulated in the outer peripheral tube. The gas pressure (P_g) inside the reactor can be calculated by enforcing the continuity equation. Also, the velocities in the respective directions can be calculated using Darcy's equation.

The continuity equation for hydrogen gas can be written as follows:

$$\varepsilon \frac{\partial(\rho_g)}{\partial t} + \nabla(\rho_g u_g) = \dot{m}_{H_2} \quad (4)$$

Momentum equation for calculating the velocity of hydrogen gas in the porous zone is determined using Darcy's equation.

$$\vec{u}_g = -\frac{K}{\mu_g}\nabla P_g \quad (5)$$

Assuming hydrogen as an ideal gas, so the density of hydrogen can be defined as

$$\rho_g = \frac{M_g P_g}{R_g T_g} \quad (6)$$

Table 3 – Thermodynamic properties of chosen materials.

Alloys	Absorption Enthalpy (kJ/mol)	Desorption Enthalpy (kJ/mol)	Absorption Entropy (J/mol K)	Desorption Entropy (J/mol K)
$La_{0.9}Ce_{0.1}Ni_5$	−25.98	27.96	104	106
$Ti_{0.99}Zr_{0.01}V_{0.43}Fe_{0.99}Cr_{0.05}Mn_{1.5}$	−27.4	28.5	112	105
$MmNi_5$	−20.35	22.55	101	110
TiCrMn	−19.6	20.1	106	103

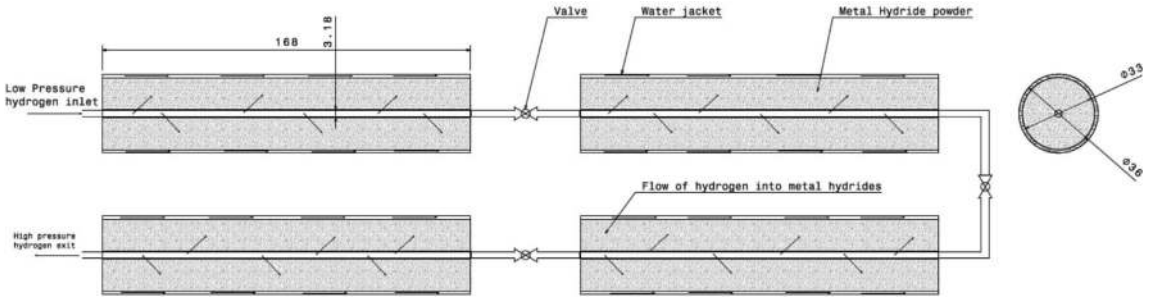

Fig. 3 – Reactor geometry.

By substituting u_g and ρ_g in Eq. (4), the gas pressure (P_g) inside the reactor is calculated using the following equation:

$$\left(\frac{\varepsilon M_g}{R_u T}\right)\frac{\partial P_g}{\partial t}+\left(\frac{\varepsilon M_g P_g}{R_u}\right)\frac{\partial}{\partial t}\left(\frac{1}{T}\right)-\frac{K}{\nu_g r}\frac{\partial}{\partial r}\left(r\frac{\partial P_g}{\partial r}\right)-\frac{K}{\nu_g}\frac{\partial}{\partial z}\left(\frac{\partial P_g}{\partial z}\right)=\dot{m}_{H_2} \tag{7}$$

The above process is continued until the hydrogen gas is filled inside the reactor (when equilibrium pressure reaches the supply pressure).

Sensible heating of MH 1 bed (Process 1′ to 2)
During this process, only heat transfer takes place between the reactor and the respective heat transfer fluid at approximately 373 K.

$$(\rho C_p)_e\frac{\partial T}{\partial t}+(\rho C_p)_g\vec{u}.\nabla T=\lambda_e\nabla^2 T \tag{8}$$

From the above equation, when the temperature of the metal hydride bed increases the hydrogen pressure also increases. For multi-stage hydrogen compression, this system is coupled with the series of reactors in such a way that the metal hydrides are filled in the reactors that the equilibrium pressure of the previous hydride alloy is higher than the equilibrium pressure of the next stage hydride alloy for the same operating temperature ranges.

Hydrogen transmission between couple reactors (Processes 2 to 3, 4 to 5 and 6 to 7)
The amount of hydrogen desorbed from the low-pressure reactor is estimated using the following equation:

$$\dot{m}_{LT}=C_d\exp\left(\frac{-E_d}{R_u T_{LT}}\right)\left(\frac{P_{eq,LT}-P_{g,t+\delta t}}{P_{eq,LT}}\right)\rho_{m,LT} \tag{9}$$

Hydrogen desorption takes place from a low-pressure reactor when there is a sufficient pressure difference between low pressure and high-pressure reactors. Due to the assumption of local thermal equilibrium between the hydrogen and the hydride bed, a combined energy equation is considered for predicting the temperature in the reaction bed:

$$(\rho C_P)_e\frac{\partial T}{\partial t}+(\rho C_P)_g\vec{u}.\nabla T=\lambda_e\nabla^2 T-\dot{m}_{LT}\left[\frac{\Delta H}{M_g}-T(C_{p,g}-C_{p,m})\right] \tag{10}$$

Simultaneously, the variations in hydrogen concentration and bed temperature of high-pressure metal hydrides (Processes 3 to 3′, 5 to 5′ and 7 to 7′) are predicted using equations (1)–(3). The variations in gas pressure during these processes in all the reactors are estimated using equation (7).

Sensible heating and cooling of high pressure and low-pressure reactors and respectively
Here, equation (8) can be used to determine the variation in beds temperature during sensible heating of high-pressure beds from 298 K to 373 K (processes 3′ to 4, 5′ to 6 and 7′ to 8) and sensible cooling of low-pressure beds from 373 K to 298 K (processes 2′ to 1, 4′ to 3 and 6′ to 5).

Compressed hydrogen delivery (Process 8 to 8′)
Finally, the compressed hydrogen is desorbed to the delivery tank by merely opening the control valve. After that, by sensible cooling of the high-pressure reactor from 373 K to 298 K (8′ to 7) the system is ready for the next cycle.

Boundary conditions of desorbing beds at T_h absorbing beds at T_l
At the end of each sensible heating process, the corresponding reactor is at desorbing condition, i.e. at T_h. The opening temperature and density of alloy powder are assumed constant in the entire reactor. The initial conditions for MH beds at T_h are:

$$\rho_{m,\,Des}(z,r)=\rho_{ss};\,T_m(z,r)=T_g(z,r)=T_{Des}=T_c;\,x_{Des}(z,r)=x_{Des,\max}$$

For absorbing beds:

$$\rho_m(z,r)=\rho_i;\quad T_m(z,r)=T_g(z,r)=T_{Abs}=T_m;\quad x(z,r)=x_{Abs,\min}$$

$$\frac{\partial T}{\partial z}(z,r,t)_{z=0}=0;\frac{\partial T}{\partial z}(z,r,t)_{z=Z}=0 \tag{8a}$$

$$P_g(z,r_i,t)=P_g \tag{9a}$$

$$-\lambda_e\frac{\partial T}{\partial r}(z,r_o,t)=U(T_{z,r_o,t}-T_f) \tag{10a}$$

where, $T_{z,ro,t}$ and T_f are the temperature of hydride bed at the outermost radius and temperature of heat transfer fluid (water), respectively. Additionally, the convective boundaries are associated with variable wall temperature conditions (equation (11)), which gives temperature change of heat transfer fluid in an axial direction. This variable wall temperature influences the average bed temperature significant, which leads to the actual condition of the system.

$$\dot{m}_w C\left(T_{w_{in}} - T_{w_{out}}\right) = U\left(T_{w_{in}} - T_{r_0}\right) \tag{11}$$

The gas pressure $P_{g,t+\delta t}$ for connecting pipes is calculated as

$$P_{g+\delta t} = \frac{n_{g+\delta t} R_u T_{g+\delta t}}{V_{Des} + V_{Abs} + V_P} \tag{12}$$

Thermal resistive network

The heat and hydrogen transfer behaviours of multi-stage SHC are studied for 0.5 kg of alloys mass in the cylindrical reactors embedded with cooling water jackets. The heat transfer from MH bed to cooling water was analysed using the thermal circuit, as shown in Fig. 4 (front and side view). With the help of this resistance network, the heat transfer rate is analysed using the following equation [54]:

$$\dot{Q} = \frac{\Delta T}{R_{t,Total}} \tag{13}$$

Here, the total thermal resistance (for conduction, convection and fins) can be calculated as

$$R_{conduction} = \frac{\ln \frac{r_2}{r_1}}{2\,\pi\,k\,L} \tag{14}$$

$$R_{convection} = \frac{1}{h\,2\,\pi\,r_2\,L} \tag{15}$$

In equation (14), r_2 and r_1 are the external and internal radius of the reactor, L is bed length, and k is thermal conductivity. In equation (15), h is the convective heat transfer coefficient.

Solution scheme

The steps involved in the solution of governing equations about heat and mass transfer behaviour of MH beds are presented in Fig. 5. Very first the properties of metal hydrides, i.e. ΔH, ΔS, ϕ, β, x_f, C_d, E_d, ρ_m and ρ_{ss}, required as input for governing equations are experimentally measured as well as occupied from literature. After that, grid size and, first input data for hydrogen concentration, alloy thermodynamic and thermo-physical properties, operating temperature, cycle period, time steps, etc. are defined. The computational domain of half of the reactor was divided into 41 × 41 grid size for obtaining the numerical solution of governing equations using a finite volume approach. After assigning the initial conditions, the MH bed pressures are calculated using the van't Hoff equation, and these values are used for the estimation of hydrogen transmission at each time steps. In the next step, energy equation, i.e. equation (10) is discretised as well as assigned the required initial and boundary conditions and solved using TDMA algorithm, which results in the average MH bed temperature. Similarly, the pressure equation is discretised and solved to generate succeeding pressure value. This newly generated pressure value is used to estimate velocity for the present time step. The simulation was continued till the present time step reaches to predefined cycle time by updating the calculated data values.

Thermodynamic performance

The thermodynamic performance, i.e. compressor work, total heat supplied and compressor efficiency is calculated using the following equations.

The compression work is calculated as

$$\begin{aligned} W_c = {} & \frac{\gamma}{\gamma-1} m_{H_{2_{(stage-1)}}} T_{abs} \left[\frac{R}{M_{H_2}}\right] \left[\left(\frac{P_{d_{(stage-1)}}}{P_{s_{(stage-1)}}}\right)^{\frac{\gamma-1}{\gamma}} - 1\right] + \\ & \frac{\gamma}{\gamma-1} m_{H_{2_{(stage-2)}}} T_{abs} \left[\frac{R}{M_{H_2}}\right] \left[\left(\frac{P_{d_{(stage-2)}}}{P_{s_{(stage-2)}}}\right)^{\frac{\gamma-1}{\gamma}} - 1\right] + \\ & \frac{\gamma}{\gamma-1} m_{H_{2_{(stage-3)}}} T_{abs} \left[\frac{R}{M_{H_2}}\right] \left[\left(\frac{P_{d_{(stage-3)}}}{P_{s_{(stage-3)}}}\right)^{\frac{\gamma-1}{\gamma}} - 1\right] + \\ & \frac{\gamma}{\gamma-1} m_{H_{2_{(stage-4)}}} T_{abs} \left[\frac{R}{M_{H_2}}\right] \left[\left(\frac{P_{d_{(stage-4)}}}{P_{s_{(stage-4)}}}\right)^{\frac{\gamma-1}{\gamma}} - 1\right] \end{aligned} \tag{16}$$

The total heat supplied is calculated as

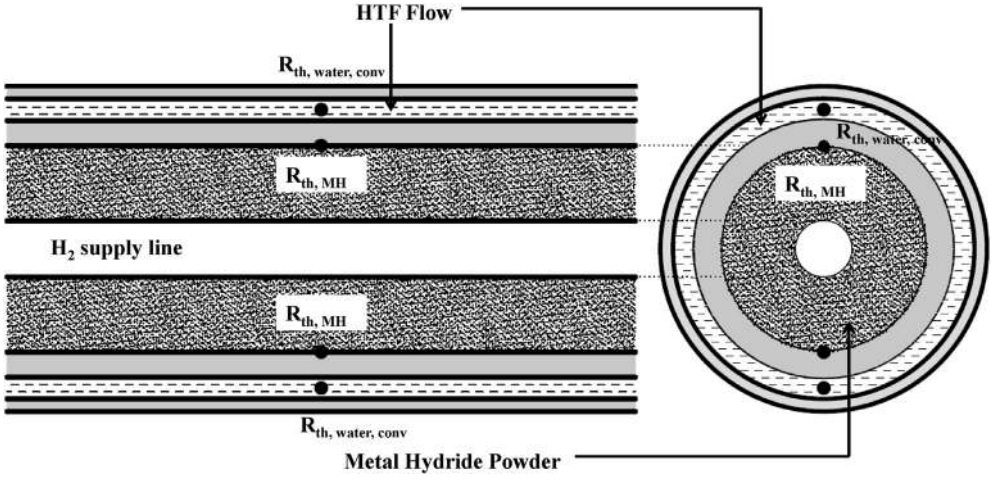

Fig. 4 – Schematic of a thermal resistance network.

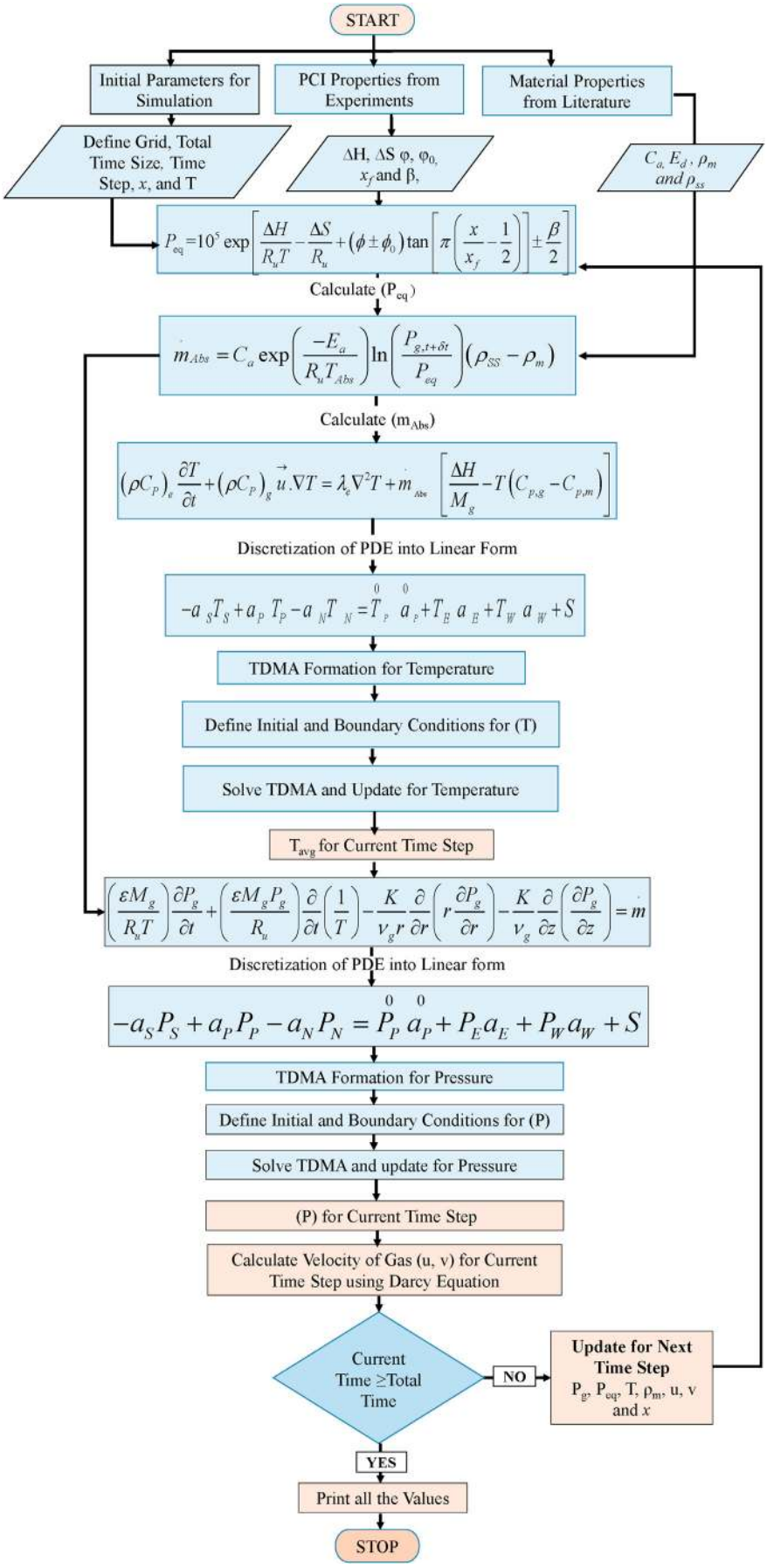

Fig. 5 – Solution scheme [55].

$$Q_h = n_{(stage-1)}\Delta H_{des_{(stage-1)}} + \left[(m_{alloy}C_{alloy} + m_R C_R)(T_{des} - T_{abs})\right] + n_{(stage-2)}\Delta H_{des_{(stage-2)}} + \left[(m_{alloy}C_{alloy} + m_R C_R)(T_{des} - T_{abs})\right] + n_{(stage-3)}\Delta H_{des_{(stage-3)}} + \left[(m_{alloy}C_{alloy} + m_R C_R)(T_{des} - T_{abs})\right] + n_{(stage-4)}\Delta H_{des_{(stage-4)}} + \left[(m_{alloy}C_{alloy} + m_R C_R)(T_{des} - T_{abs})\right] \quad (17)$$

The compression efficiency is calculated as

$$\eta_c = \frac{Isentropic\ compression\ work}{Total\ heat\ input\ to\ compressor} = \frac{W_c}{Q_h} \quad (18)$$

Results and discussion

The results obtained from the performance investigation of multi-stage sorption hydrogen compressor in terms of variations in bed pressure, temperature and concentration are discussed in following sub-sections.

Model validation

The numerical model is validated for MH bed temperature as well as hydrogen concentration at a hydrogen supply pressure of 10 bar and operating temperature of 30 °C, as shown in Fig. 6. For validation purpose, the reactor geometry is considered the same as used in experimental studies [9], i.e. 130 mm length and 30 mm inner diameter. The metal hydride used is $La_{0.8}Ce_{0.2}Ni_5$ with a total mass of 0.25 kg as well as the other material properties are similar to presented in Ref. [9].

Figure 6 shows the variation of MH bed temperature and hydrogen concentration obtained from both experimental measurement [9] and numerical estimation. It is observed that the variation in temperature and concentration generated through numerical modelling are in good agreement with experimentally measured values. There is a small deviation occurred at the peak point of the temperature curve, which is due to the fast reaction kinetics of metal hydride resulted from high-pressure difference at the beginning. This may be difficult to incorporate with numerical results. In the case of hydrogen concentration, it is observed that the full concentration reached in 470 s in experimentation whereas it reached in 230 s in simulation. The deviation may be due to the experimental uncertainties as well as several assumptions in a numerical model. It is also observed that about 90% of hydrogen transmission is achieved within 80 s in experimentation and within 50 s in simulation. The results obtained in Fig. 6 revealed the suitability of the generated numerical model for the prediction of hydrogen compressor performance. The performance prediction of multi-stage hydrogen compressor is carried out employing the same numerical code by incorporating certain adjustments to lodge the staging. The dimension and schematic of the reactor used in present work are already presented in Section Metal hydride reactor.

PCIs of metal hydrides

The PCIs of $La_{0.9}Ce_{0.1}Ni_5$, $Ti_{0.99}Zr_{0.01}V_{0.43}Fe_{0.99}Cr_{0.05}Mn_{1.5}$, $MmNi_5$ and TiCrMn alloys are presented in Fig. 7 at the absorption temperature of 298 K and a desorption temperature of 373 K. Since the thermodynamic system works within the plateau region, the PCIs of the materials are presented only for the plateau phase.

It is seen from PCIs that the equilibrium pressures of all the desorbing alloys are much higher than the corresponding absorbing alloys in coupled MH beds. This proves the suitability of these alloys for better performance of SHC because it allows complete absorption and desorption of hydrogen, which in return favourable for system performance. Also, it is seen that the pressures at the end of absorption processes are higher than that of the beginning. This is due to the existence of a plateaued slope that results from the presence of impurities or surface contaminations. In general, the presence of high plateau slope is not acceptable for the development of thermal devices, but in case of hydrogen compressor, it is somehow favourable because, at the end of sensible heating of the bed, this results in high discharge pressure. However, it is to be noted that the higher plateau slope leads to a reduction in reversible hydrogen storage capacity. In this system with the implementation of multi staging, it is observed that the $La_{0.9}Ce_{0.1}Ni_5$ absorbs hydrogen at 9.5 bar and 298 K and TiCrMn delivers the high-pressure hydrogen at 695 bar and 373 K. This observation leads to the maximum compression

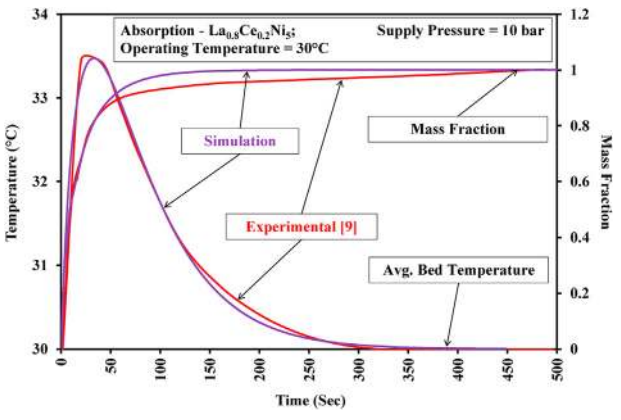

Fig. 6 – Model validation for average MH bed temperature and hydrogen concentration factor.

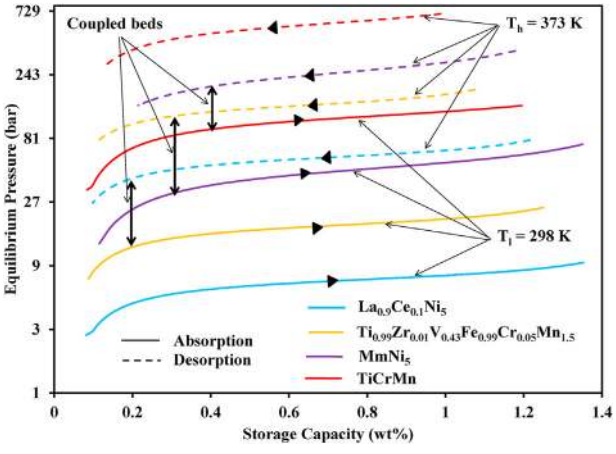

Fig. 7 – PCIs of MH beds at absorption and desorption temperatures.

ratio of 73.15 by considering the endpoints of the plateau regions of $La_{0.9}Ce_{0.1}Ni_5$ and TiCrMn hydrides.

Thermodynamic cycle with pressure variations

Figure 8 shows the thermodynamic cycle represented on the van't Hoff plot constructed using mid-plateau pressures of employed metal hydrides. In this thermodynamic cycle, the actual variation of MH pressures is also presented for all the processes in respect of PCIs. It is already discussed in Section Working principle of multi-stage sorption hydrogen compressor that the sorption hydrogen compressor works within the plateau region as well as its representation in the thermodynamic cycle. Similarly, the thermodynamic cycle in Fig. 8 is constructed using the data from Fig. 7. The state points $P_{i,1}$, $P_{i,2}$ and $P_{i,3}$ are the intermediate pressure at which the hydrogen transmission stops where pressure equilibrium reached. The details of MH bed conditions, i.e. the opening pressure and discharge pressure corresponding to storage capacities (wt%) for all the stages are presented in Table 4. It also shows the values of a maximum pressure difference between coupled reactors concerning mid-plateau pressures as well as plateau region end to endpoints, i.e. the pressure gap between the starting point of a desorbing alloy ($\beta \rightarrow \alpha+\beta$) and stating point of absorbing alloy ($\alpha \rightarrow \alpha+\beta$).

It can be seen that high-pressure differences exist among the coupled reactors in respect of both mid-plateau as well as ends of the plateau region, and increased values are obtained for subsequent stages. Also, the minimum of 68.37 bar and maximum of 313.93 bar gaps are obtained among coupled beds that lead to high reaction rates, which is discussed in subsequent sections. The obtained data also depicts that the maximum discharge pressure of 695.34 bar can be achieved at the end of sensible heating of TiCrMn. This high-pressure output at the temperature of 373 K is the outcome of the selection of $La_{0.9}Ce_{0.1}Ni_5$ in the first stage because this material provides excellent pressure lift with a small upsurge in temperature with significant reversible hydrogen storage capacity, and favourable plateau slope and hysteresis. However, the materials used in the present study provide high-pressure lift and excellent PCI properties in the reported literature.

Variation in MH beds temperature

It is well known that the absorption and desorption of hydrogen by metal hydrides are exothermic and endothermic reactions, respectively. Therefore, in the present system, wherever hydrogen absorption takes place, a certain amount of heat is released whereas a certain amount of heat is supplied to the system for hydrogen desorption. This phenomenon is seen in Fig. 9 with the sudden drop and rise in MH bed temperatures at each stage.

In Fig. 9, the increase in $La_{0.9}Ce_{0.1}Ni_5$ bed temperature during hydrogen absorption at 298 K and sensible heating from 298 K to 373 K can be seen at the stage − 1 whereas for stage − 2, the temperature variation in coupled beds, i.e. $La_{0.9}Ce_{0.1}Ni_5$ and $Ti_{0.99}Zr_{0.01}V_{0.43}Fe_{0.99}Cr_{0.05}Mn_{1.5}$ during desorption followed by sensible cooling and absorption followed by sensible heating, respectively, is presented. Similarly, it is shown for other MH beds for stage − 3, stage − 4 and hydrogen delivery processes. The sudden rise and drop in bed temperatures are due to the fast reaction rates, which results from the high-pressure difference between beds. Due to this, in the beginning, hydrogen transmission is fast, and then it decreases with a decrease in pressure differential. It can be seen that the bed temperature first increased then decreased gradually to its original temperature, i.e. 298 K during absorption similarly, during desorption the bed temperature suddenly drops then increased gradually to 373 K due to the circulation of heat transfer fluid in the annulus. The values of maximum rise and drop in bed temperatures for all the stages are given in Table 5. These temperature jumps are also due to

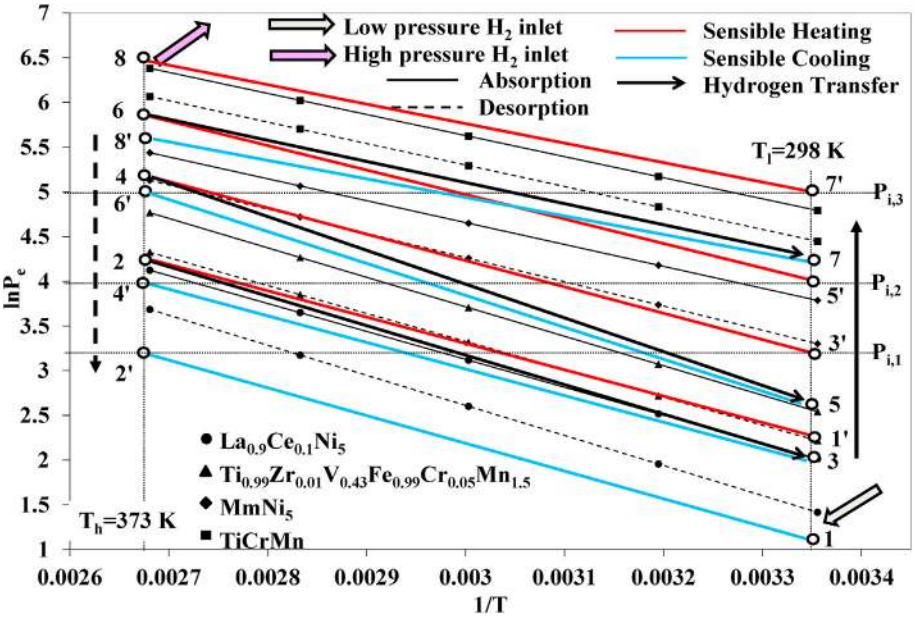

Fig. 8 – Thermodynamic cycle presenting the pressure variation during processes.

Table 4 – MH bed conditions during hydrogen transfer processes.

Compression Stages	MH beds condition		Pressure Differential w.r.t Mid Plateau (bar)	Maximum Pressure Differential w.r.t PCIs(bar)
	Desorptionpoint [β→α+β]	Absorption point [α→α+β]		
Supply from low-pressure cylinder (Stage – 1)	–	$La_{0.9}Ce_{0.1}Ni_5$; 0.081 wt% and 2.7 bar at 298 K	–	Supply pressure 9.5
Stage – 2	$La_{0.9}Ce_{0.1}Ni_5$; 1.21 wt% and 78.5 bar at 373 K	$Ti_{0.99}Zr_{0.01}V_{0.43}Fe_{0.99}Cr_{0.05}Mn_{1.5}$; 0.14 wt% and 10.13 bar at 298 K	27.12	68.37
Stage – 3	$Ti_{0.99}Zr_{0.01}V_{0.43}Fe_{0.99}Cr_{0.05}Mn_{1.5}$; 1.07 wt% and 187.7 bar at 373 K	$MmNi_5$; 0.17 wt % and 20.75 bar at 298 K	31.39	166.95
Stage – 4	$MmNi_5$; 1.17 wt % and 367.13 at 373 K	TiCrMn; 0.14 wt% 53.20 bar at 298 K	48.68	313.93
Delivery to the high-pressure cylinder	TiCrMn; 0.98 wt% 695.34 bar at 373 K	–	–	Max. delivery pressure 695.34

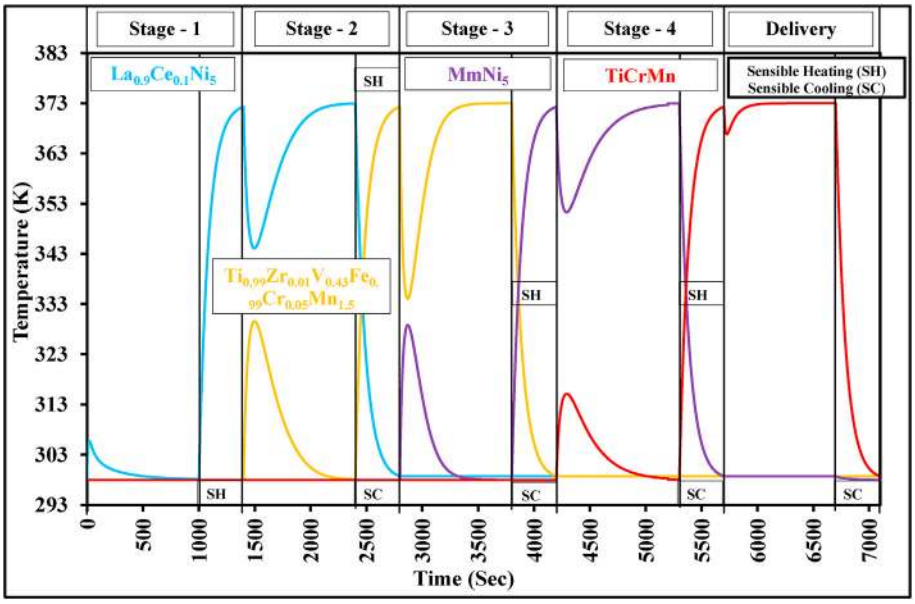

Fig. 9 – Average MH bed temperature during hydrogen transmission processes.

the accumulation of heat because of the poor thermal conductivity of metal hydride powder.

Rates of hydrogen transmission

The rates of hydrogen transmission during all the processes are presented in Fig. 10. It can be seen that full hydrogen transmission occurred within 500 s for all the stages except stage – 1. This is due to a very high-pressure difference between coupled reactors whereas, in the first stage, hydrogen is supplied to MH 1 at a pressure of 9.5 bar, which is comparatively very less with other stages. The hydrogen transmissions presented in Fig. 10, in connection with Fig. 5, evidences the transmission of a significant amount of hydrogen, which is

Table 5 – MH bed temperature variation values.

Stages	Materials	Variation in MH bed temperature	Time (sec)
Stage 1	$La_{0.9}Ce_{0.1}Ni_5$	From 298 K to 305.6 K	in 20 s
Stage 2	$La_{0.9}Ce_{0.1}Ni_5$	From 373 K to 344.1 K	in 96 s
	$Ti_{0.99}Zr_{0.01}V_{0.43}Fe_{0.99}Cr_{0.05}Mn_{1.5}$	From 298 K to 329.5 K	in 96 s
Stage 3	$Ti_{0.99}Zr_{0.01}V_{0.43}Fe_{0.99}Cr_{0.05}Mn_{1.5}$	From 373 K to 334 K	in 69 s
	$MmNi_5$	From 298 K to 328.8 K	in 68 sed
Stage 4	$MmNi_5$	From 373 K to 351 K	in 90 s
	TiCrMn	From 298 K to 315.1 K	in 93 s
Delivery	TiCrMn	From 373 K to 366.8 K	in 24 s

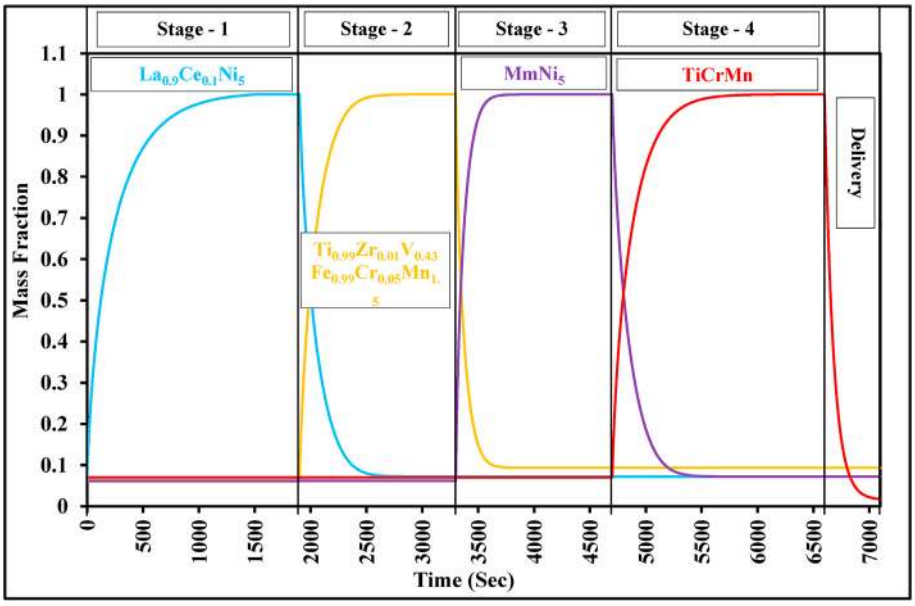

Fig. 10 – Rate of hydrogen transmission.

responsible for better system performance. The heat and mass transfer analyses of multi-stage SHC demonstrate that the overall cycle completes within 6000 s, including sensible heating and cooling processes.

MH bed pressure variations

Figure 11 shows the variation in MH bed pressure in each stage of a multi-stage sorption hydrogen compressor. The minimum pressure of the cycle is at the start of the first stage, i.e. 2.7 bar at 298 K whereas the maximum pressure of the cycle is at the end of the fourth stage, i.e. 695 bar at 373 K. The sharp peaks in the figure are the rise in bed pressure during sensible heating processes. It can be seen that the bed pressure of desorption alloy gradually decreases and the pressure of absorbing alloy increases with the progression of compression stages. The variation in bed pressure stops with the completion of hydrogen transmission, and the pressures of both alloys come in equilibrium, i.e. at an intermediate pressure. The values of opening pressure and discharge pressure for all the materials at each stage are already presented in Table 4.

Thermodynamic performance

The thermodynamic performances of multi-stage sorption hydrogen compressor are estimated for static as well as dynamic conditions. Here, the static performance stands for the performance parameters estimated using fix values of the

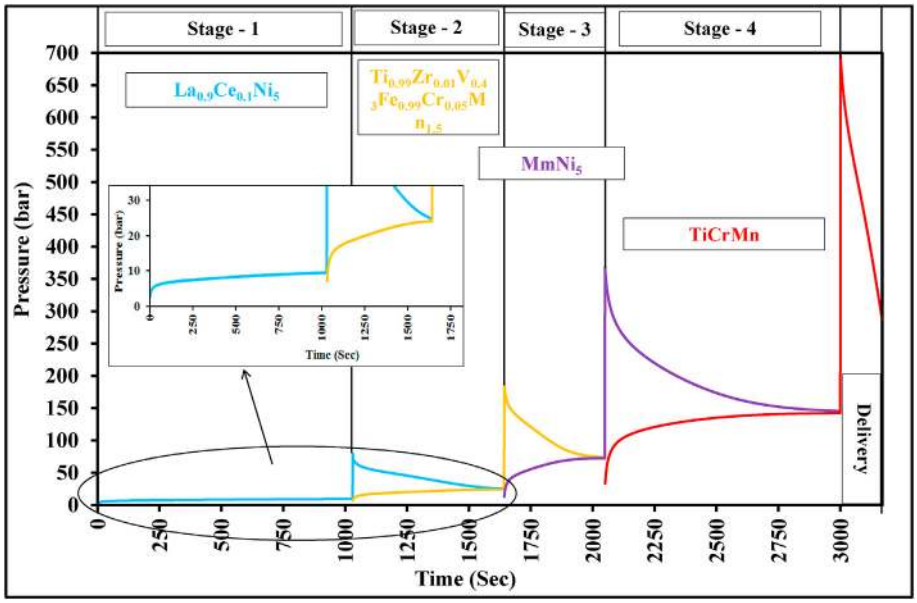

Fig. 11 – MH bed pressure variations.

mass of hydrogen transmitted, and supply and discharge pressures whereas dynamic performance stands for the performance estimation using the data generated through numerical modelling. In contrast, the other constant properties used in equations (13)–(16) are the same in both analyses. The system performance is estimated using the series of equations presented in Section Solution scheme. The estimated compressor work, heat input and efficiency for each stage through static data are given in Table 6. The values of other constants are given in the author's previous article [56]. The overall compressor work is estimated as 37.82 kJ whereas total heat input as 356 kJ with the overall efficiency of 10.26%. It is observed that compressor work is higher at stage − 1 and goes on decreasing for further stages. This is due to a decrease in pressure ratio (discharge pressure/supply pressure). A similar pattern is observed for heat input also, but this entirely depends on reversible hydrogen as well as desorption enthalpies. The compressor work decreased by 69.8%, 75.2% and 80.4% from the stage − 1 to stage − 2, stage − 3 and stage − 4, respectively whereas it decreased by 17.8% from the stage − 2 to stage − 3 and by 21% from the stage − 3 to stage − 4. Similarly, heat input is reduced by 7.6%, 17.7% and 33.6% respectively. It is also observed that at the end of the fourth stage, 5 g of hydrogen can be delivered at predicted higher pressure.

The above performance parameters are estimated for 0.5 kg of each metal hydrides. To forecast the performance of the system for higher output, the thermodynamic performance is also estimated for a large quantity of metal hydrides, i.e. 10 kg each. The overall work input is estimated as 946.7 kJ while overall heat input as 7120 kJ with maximum hydrogen discharge of ~100 g at the end of 4-stage compression. Despite these high discharge, the increased cycle time may result in the employment of 10 kg of metal hydrides due to slower reaction between hydrogen and a large quantity of alloy particles.

On the other hand, dynamic performance is estimated using the parameters generated through CFD simulation. The variation of compressor work and heat input along with the overall efficiency with the variation of hydrogen transmission are shown in Figs. 12 and 13. It can be seen that the compressor work, heat input and overall efficiency increases with the increase in the amount of hydrogen transmitted. Also, the rate of performance parameters is fast at the beginning then slows down and the compressor work reached equilibrium values of 27.14, 8.18, 6.72 and 5.3 kJ, and heat input values reached to 101.41, 96.46, 85.88 and 69.25 kJ with the overall efficiency of 13.3%.

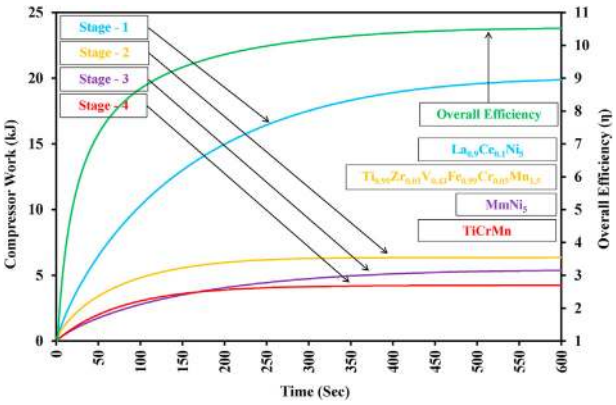

Fig. 12 − Effect of hydrogen transmission on compressor work and efficiency.

Also, the effects of discharge temperature on system performance are estimated. The discharge temperature varied from 373 K to 473 K, and its effect on compressor work, heat input and overall efficiency are studied as shown in Fig. 14. It is observed that the compressor work and overall efficiency decreases with an increase in discharge temperature, whereas the heat input increases. With an increase in discharge temperature, the higher discharge pressure can be achieved since the equilibrium pressure of metal hydride increases with operating temperature. Conversely, this leads to a significant decrease in available pressure differential between coupled reactors and results in slower reaction kinetics (increase in overall cycle time) and reduction in hydrogen exchange. From the previous experiments on metal hydrides PCIs [33,57], it was observed that with the increase in operating temperature by 20 °C, the reversible hydrogen storage capacity decreased by 3–4% and this reduction will be more at higher operating temperatures as well as leads to increased plateau slope. Therefore, in the present study, to estimate the static thermodynamic performance of the system at different discharge temperatures the reversible hydrogen storage is assumed to be reduced by 4% with an increase in temperature by 20 °C.

It can be seen from equations (16) and (17) that the compressor work as well as heat input greatly influenced by the amount of hydrogen transmission. Due to this, the decrease in compressor work is observed with an increase in discharge temperature. Moreover, the increase in heat input is due to the increase in the sensible heating amount. Both together leads to a decrease in the overall efficiency of the system.

Table 6 − Thermodynamic performance of multi-stage sorption hydrogen compressor.

Compression Stages →	Stage − 1	Stage - 2	Stage − 3	Stage - 4
Alloy	$La_{0.9}Ce_{0.1}Ni_5$	$Ti_{0.99}Zr_{0.01}V_{0.43}Fe_{0.99}Cr_{0.05}Mn_{1.5}$	$MmNi_5$	TiCrMn
Reversible Storage Capacity ($wt\%_{rev}$)	1.21	1.075	1.17	0.98
Supply Pressure (bar)	9.5	78.5	187.7	367.13
Delivery Pressure (bar)	78.5	187.7	367.13	695.34
Compressor Work; W_c (kJ)	21.68	6.53	5.37	4.23
Heat Supplied; W_h (kJ)	104.41	96.46	85.88	69.25
Efficiency; η	20.77	6.77	6.25	6.12

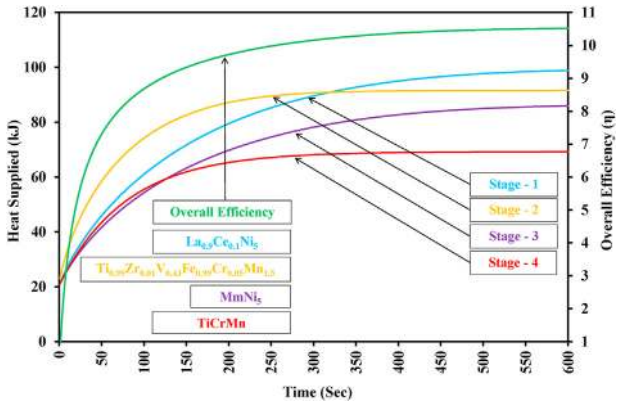

Fig. 13 – Effect of hydrogen transmission on heat input and efficiency.

Techno-economic analysis

Metal hydride based hydrogen compressor is proposed for hydrogen compression without contamination and with reasonably low energy cost that makes it an attractive alternative to the mechanical compressor. The characteristic of utilizing waste heat as an input, in case of sorption hydrogen compressor, helps in reducing operation cost significantly in comparison with mechanical hydrogen compressor. In 2018, Emmanuel et al. [58] have presented a detail discussion on the developments on sorption hydrogen compressor and early markets. A brief discussion on techno-economic analysis in connection with the previous study [58] is presented here. Table 7 presents a comparison between conventional and metal hydride based hydrogen compressor.

It is clear from the above table that the sorption hydrogen compressor possesses substantial benefits over mechanical hydrogen compressor in terms of lower weight, lower capital cost, lower operation and maintenance cost as well as it operates using waste heat (190 lit/min @ 90 °C). Sorption hydrogen compressor can be directly introduced to business like chemical industry (for utilizing waste heat), hydrogen refuelling stations and renewable energy source (RES) storage in compressed hydrogen. The better target market for sorption hydrogen compressor is its incorporation in a self-sufficient power system running through RES and hydrogen systems. It is concluded form the techno-economic analysis that the sorption hydrogen compressor possessed good commercialisation potential. This is due to the requirement of renewable energy systems in central Europe as a result of the

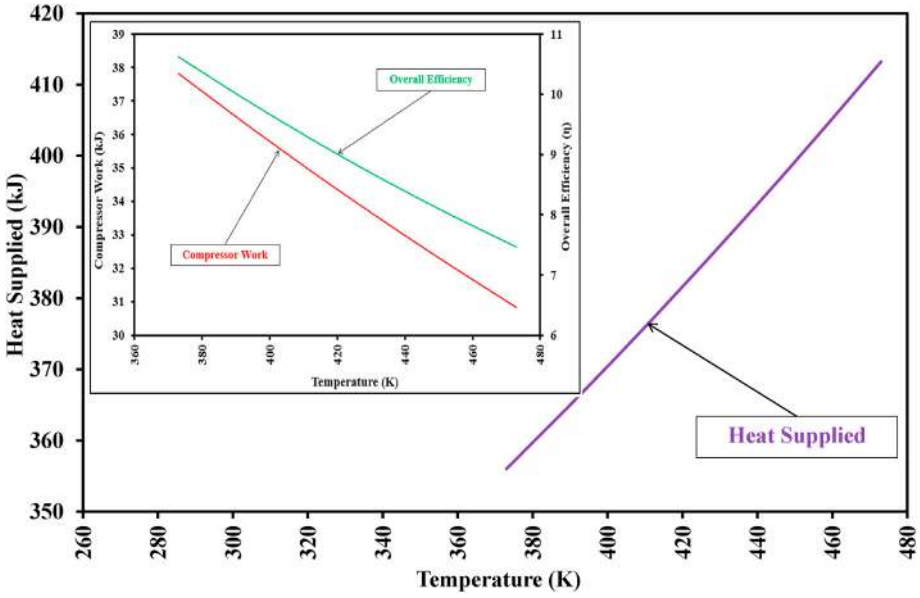

Fig. 14 – Effect of discharge temperature on heat input, compressor work and efficiency.

Table 7 – Comparison between mechanical and sorption hydrogen compressor [58].

S.No.	Parameters	Sorption Hydrogen Compressor	Mechanical Hydrogen Compressor
1	Hydrogen Discharge (Nm^3/h)	56.63	56.63
2	Supply Pressure (bar)	6.89	6.89
3	Discharge Pressure (psia)	248.2	248.2
4	No. of Stages	5	3
5	Total Weight (kg)	1000	3600
6	Electric Power Required (W)	500	20,000
7	Estimated Capital Cost (Euro)	130,000	145,000
8	Annual Power Cost (2000 h/y, €0.1/kWh)	100	4000
9	Annual Maintenance Cost (€)	1000	8000

exclusion of nuclear plants. Also, in Europe, the number of hydrogen refuelling stations are increasing as well as several hydrogen-powered vehicles are introduced in the market.

In 2020, Lototskyy et al. [23] have presented the detailed technical and economical analyses of three years operation of the hydrogen refuelling station. It is reported that 25% of the total cost of refuelling station goes to the development of sorption hydrogen compressor. It is also reported that the capital, as well as operation costs, are significantly lower than the existing hydrogen refuelling stations. It can be observed from the above discussion, and Table 7 that for the similar pressure output, the total estimated cost of sorption hydrogen compressor is significantly lower than the mechanical compressor. The estimated capital cost for five-stage sorption hydrogen compressor for the pressure output of 248.2 psia is 130,000 €. The comparable capital cost can be expected for the four-stage sorption hydrogen compressor proposed in the present study with the pressure output of >500 bar.

Conclusions

The performance investigation of multi-stage sorption hydrogen compressor through a finite volume approach at operating temperatures of 298 K and 373 K led to the following conclusions:

1. A new multi-stage sorption hydrogen compressor is proposed and analysed its performance for the compression of low-pressure hydrogen at a supply pressure of 9.5 bar, 298 K to high-pressure hydrogen discharge of more than 500 bar at 373 K with the employment of $La_{0.9}Ce_{0.1}Ni_5$, $Ti_{0.99}Zr_{0.01}V_{0.43}Fe_{0.99}Cr_{0.05}Mn_{1.5}$, $MmNi_5$ and TiCrMn, which results from the screening of several metal hydrides.
2. The solution scheme adopted for CFD simulation of multi-stage SHC is presented. The simulation predicted the behaviour of MH bed temperature, pressure and hydrogen transmission during compression stages. The overall cycle time is predicted as 6000 s, including compression stages, and sensible heating and cooling.
3. The thermodynamic cycle of multi-stage SHC is constructed showing the actual variation in MH bed pressure corresponding to PCIs are presented, yields better understanding of the availability of maximum pressure differential among coupled reactors, which results in fast kinetics and maximum hydrogen transfer.
4. The static performance of SHC yields the maximum compression work of 37.82 kJ and total heat supply of 356 kJ with the cycle efficiency of 10.62%. The dynamic performance is estimated with the employment of predicted MH bed parameters, which demonstrates that the system performance (compressor work, total heat input and overall efficiency) increases with hydrogen transmission rate and amount.
5. The increase in discharge temperature on system performance results into increase in heat input, whereas a decrease in compressor work and cycle efficiency.
6. The maximum pressure ratio from the start of the first stage to the end of the fourth stage is obtained to be 257, i.e. from 2.7 bar to 695 bar with the discharge of 5 g of hydrogen by using 0.5 kg of each alloy whereas the implementation of 10 kg of metal hydrides results in a discharge of 100 g of hydrogen.
7. The proposed system and methodology can be employed for very high-pressure hydrogen output by varying discharge temperature and corresponding working pairs. The main advantage of such systems is its ability to operate using low-grade heat energy. In contrast, the main disadvantage may be the requirement of more number of stages and operation time to produce the pressure output like conventional hydrogen compressor. Moreover, the estimated capital and operation costs of a sorption system are lower than that of a mechanical compressor.

Declaration of competing interest

The authors declare that they have no known competing financial interests or personal relationships that could have appeared to influence the work reported in this paper.

REFERENCES

[1] Mueller WM, Blackledge JP, Libowitz GG. Metal hydrides. New York: Academic Press; 1968.
[2] Lc Beavis. Characteristics of some binary transitional metal. J Less Common Met 1969;19:315–28.
[3] Northrup Jr CJM, Heckes AA. A hydrogen-actuated pump. J Less Common Met 1980;74:419–26.
[4] Wang Y, Zheng L, Yang F, Meng X, Zhang Z. Performance comparison and analysis of typical energy conversion Cycle. In: 2011 international conference on computer distributed control and intelligent environmental monitoring. IEEE; 2011. p. 1603–6.
[5] Muthukumar P, Prakash Maiya M, Srinivasa Murthy S. Performance tests on a thermally operated hydrogen compressor. Int J Hydrogen Energy 2008;33:463–9.
[6] Muthukumar P, Prakash Maiya M, Srinivasa Murthy S. Experiments on a metal hydride based hydrogen compressor. Int J Hydrogen Energy 2005;30:879–92.
[7] Muthukumar P, Prakash Maiya M, Srinivasa Murthy S. Parametric studies on a metal hydride based single stage hydrogen compressor. Int J Hydrogen Energy 2002;27:1083–92.
[8] Muthukumar P, Singh Patel Kishore, Sachan Pratik, Singhal Nished. Computational study on metal hydride based three-stage hydrogen compressor. Int J Hydrogen Energy 2012;37:3797–806.
[9] Yogesh Madaria E, Kumar Anil. Effect of heat transfer enhancement on the performance of metal hydride based hydrogen compressor. Int J Hydrogen Energy 2016;41:3961–73.
[10] Vinod Kumar Sharma, Anil Kumar E. Thermodynamic analysis of two stage metal hydride based hydrogen compressor. Mater Today Proc 2018;5:23218–23.
[11] Karagiorgis G, Christodoulou CN, Storch HV, Tzamalis G, Deligiannis K, Hadjipetrou D, Odysseos M, Roeb M, Sattler C. Design, development, construction and operation of a novel metal hydride compressor. Int J Hydrogen Energy 2017;42:12364–74. https://doi.org/10.1016/j.ijhydene.2017.03.195.

[12] Pearson D, Bowman R, Prina M, Wilson P. The Planck sorption cooler: using metal hydrides to produce 20K. J Alloys Compd 2007;446–447:718–22.
[13] Wang XH, Bei YY, Song XC, Fang GH, Li SQ, Chen CP, et al. Investigation on high-pressure metal hydride hydrogen compressors. Int J Hydrogen Energy 2007;32:4011–5.
[14] Li H, Wang X, Dong Z, Xua L, Chen C. A study on 70 MPa metal hydride hydrogen compressor. J Alloys Compd 2010;502:503–7. https://doi.org/10.1016/j.jallcom.2010.04.206.
[15] Hopkins RR, Kim KJ. Hydrogen compression characteristics of a dual stage thermal compressor system utilising LaNi5 and Ca0.6Mm0.4Ni5 as the working metal hydrides. Inter J Hydro Energy 2010;35:5693–702. https://doi.org/10.1016/j.ijhydene.2010.03.065.
[16] Cieslik J, Kula P, Filipek SM. Research on compressor utilising hydrogen storage materials for application in heat treatment facilities. J Alloys Compd 2009;480:612–6.
[17] Bhuiya MH, Lee CY, Hopkins R, Yoon H, Kim S, Park SH, et al. A high-performance dual-stage hydrogen compressor system using Ca0.2Mm0.8Ni5 metal hydride. ASME; 2011. 2011 Conf on smart materials, adaptive structures and intelligent systems, SMASIS2011.
[18] Laurencelle F, Dehouche Z, Goyette J, Bose TK. Integrated electrolyser-metal hydride compression system. Inter J Hydog Energy 2006;31:762–8. https://doi.org/10.1016/j.ijhydene.2005.06.019.
[19] Laurencelle F, Dehouche Z, Morin F, Goyette J. Experimental study on a metal hydride based hydrogen compressor. J Alloys Compd 2009;475(1–2):810–6. https://doi.org/10.1016/j.jallcom.2008.08.007.
[20] Galvis AR, Leardini F, Bodega J, Ares JR, Fernandez JF. Realistic simulation in a single stage hydrogen compressor based on AB2 alloys. Int J Hydrogen Energy 2016;41:9780–8. https://doi.org/10.1016/j.ijhydene.2016.01.125.
[21] Galvis AR, Leardini F, Ares JR, Cuevas F, Fernandez JF. Simulation and design of a three-stage metal hydride hydrogen compressor based on experimental thermodynamic data. Int J Hydrogen Energy 2018;43:6666–76. https://doi.org/10.1016/j.ijhydene.2018.02.052.
[22] Goshome Kiyotaka, Endo Naruki, Tetsuhiko Maeda. Evaluation of a BCC alloy as metal hydride Evaluation of a BCC alloy as metal hydride hydrogen apparatus. Int J Hydrogen Energy 2019;44:10800–7.
[23] Lototskyy Mykhaylo, Davids Moegamat Wafeeq, Swanepoel Dana, Louw Gerhard, Klochko Yevgeniy, Smith Fahmida, Haji Fatema, Tolj Ivan, Chidziva Stanford, Pasupathi Sivakumar, Linkov Vladimir. Hydrogen refuelling station with integrated metal hydride compressor: layout features and experience of three-year operation. Int J Hydrogen Energy 2020;45:5415–29.
[24] Minko Konstantin B, Bocharnikov Mikhail S, Yanenko Yurii B, Lototskyy Mykhaylo V, Kolesnikov Andrei, Tarasov Boris P. Numerical and experimental study of heat-and-mass transfer processes in two-stage metal hydride hydrogen compressor. Int J Hydrogen Energy 2018;43:21874–85.
[25] Gkanas EI, Khzouz M. Numerical analysis of candidate materials for multi-stage metal hydride hydrogen compression processes. Renew Energy 2017;111:484–93. https://doi.org/10.1016/j.renene.2017.04.037.
[26] Gkanas EI, Christodoulou CN, Tzamalis G, Stamatakis E, Chroneos A, Deligiannis K, Karagiorgis G, Stubos AK. Numerical investigation on the operation and energy demand of a seven-stage metal hydride hydrogen compression system for hydrogen refuelling stations. Renew Energy 2020;147:164–78.
[27] Dehouche Z, Grimard N, Laurencelle F, Goyette J, Bose TK. Hydride alloys properties investigations for hydrogen sorption compressor. J Alloys Compd 1999;399:224–36.
[28] Khyzhun OY, Lototsky MV, Riabov AB, Rosenkilde C, Yartys VA, Jorgensen S, Denys RV. Sn-containing (La, Mm) Ni5– xSnxH5– 6 intermetallic hydrides: thermodynamic, structural and kinetic properties. J Alloys Compd 2003;356:773–8.
[29] Singh RK, Gupta BK, Lototsky MV, Srivastava ON. On the synthesis and hydrogenation behaviour of $MmNi_{5-x}Fe_x$ alloys and computer simulation of their P–C–T curves. J Alloys Compd 2004;373:208–13.
[30] Kumar E Anil, Prakash Maiya M, Srinivasa Murthy S, Viswanathan B. Structural, hydrogen storage and thermodynamic properties of some mischmetal–nickel alloys with partial substitutions for nickel. J Alloys Compd 2009;476:92–7.
[31] Odysseos M, De Rango P, Christodoulou CN, Hlil EK, Steriotis T, Karagiorgis G, Charalambopoulou G, Papapanagiotou T, Ampoumogli A, Psycharis V, Koultoukis E, Fruchart D, Stubos A. The effect of compositional changes on the structural and hydrogen storage properties of (La–Ce)Ni5 type intermetallics towards compounds suitable for metal hydride hydrogen compression. J Alloys Compd 2013;580:S268–70.
[32] Romanov IA, Borzenko VI, Kazakov AN. Influence of high thermal conductivity addition on PCT isotherms of hydrogen storage alloy. IOP Conf Series: J Phys 2018;1128:012105.
[33] Sharma, Kumar Vinod, Kumar E Anil. Studies on La based intermetallic hydrides to determine their suitability in metal hydride based cooling systems. Intermetallics 2015;57:60–7.
[34] Liang G, Hout J, Schulz R. Hydrogen storage properties of the mechanically alloyed LaNi -based5 materials. J Alloys Compd 2001;320:133–9.
[35] Vinod Kumar Sharma, Anil Kumar E, Prakash Maiya M, Srinivasa Murthy S. Experimental and theoretical studies on static and dynamic pressureeconcentration isotherms of MmNi5-xAlx (x = 0, 0.3, 0.5 and 0.8) hydrides. Int J Hydrogen Energy 2014;39:18940–51.
[36] Popeneciu G, Almasan V, Coldea I, Lupu D, Misan I, Ardelean O. Investigation on a three-stage hydrogen thermal compressor based on metal hydrides. J Phys: Conf Series 2009;182:012053.
[37] Karthick Selvam P, Muthukumar P, Linder M, Mertz R, Kulenovic R. Measurement of thermochemical properties of some metal hydrides e Titanium (Ti), misch metal (Mm) and lanthanum (La) based alloys. Int J Hydrogen Energy 2013;38:5288–301.
[38] Muthukumar P, Maiya MP, Murthy SS. Experiments on a metal hydride-based hydrogen storage device. Int J Hydrogen Energy 2005;30:1569–81.
[39] P Muthukumar, Umekar Manvendra M. Study of coupled heat and mass transfer during absorption of hydrogen in MmNi4·6Al0·4 based hydrogen storage device. Sadhana 2009;34:255–70.
[40] Dewan Anupam, Muthukumar P, Satheesh A, Madhavakrishna U, Dewan A. Numerical investigation of coupled heat and mass transfer during desorption of hydrogen in metal hydride beds. Energy Convers Manag 2009;50:69–75.
[41] Borzone EM, Baruj A, Blanco MV, Meyer GO. Dynamic measurements of hydrogen reaction with LaNi5-xSnx alloys. Int J Hydrogen Energy 2013;38:7335–43.
[42] Lototsky MV, Yartys VA, Pollet BG, Bowman Jr RC. Metal hydride hydrogen compressors: a review. Int J Hydrogen Energy 2014;39:5818–51.

[43] Satya Sekhar B. Design of a AB2-metal hydride cylindrical tank for renewable energy storage. J Energy Stor 2017;14:203–10.
[44] Satheesh A, Muthukumar P. Performance investigations of a single-stage metal hydride heat pump. Int J Hydrogen Energy 2010;35:6950–8.
[45] Zhou Z, Zhang J, Ge J, Feng F, Dai Z. Mathematical modeling of the PCT curve of hydrogen storage alloy. Int J Hydrogen Energy 1994;19:269–73.
[46] Beeri O, Cohen D, Gavra Z, Johnson JR, Mintz MH. Thermodynamic characterisation and statical thermodynamics of the TiCrMn - H2 (D2) system. J Alloys Compd 2000;299:217–26.
[47] Visaria M, Mudawar I, Pourpoint T. Enhanced heat exchanger design for hydrogen storage using high-pressure metal hydride–Part 2. Experimental results. Int J Heat Mass Tran 2011;54:424–32.
[48] Pickering L, Reed D, Bevan AI, Book D. Ti–V–Mn based metal hydrides for hydrogen compression applications. J Alloys Compd 2015;645:S400–3.
[49] Sekhar BS, Pailwan SP, Muthukumar P. Studies on metal hydride based single-stage heat transformer. Int J Hydrogen Energy 2013;38:7178–87.
[50] Singh RK, Gupta BK, Lototsky MV, Srivastava ON. (La, Mm) Ni5–x Fe xH6-7 Intermetallic hydrides: thermodynamic structural and hydrogen absorption properties and computer simulation studies of P–C–T isotherms. Lyon France: WHEC; 2006.
[51] Paya J, Linder M, Laurien E, Corberan JM. Mathematical models for the P–C–T characterization of hydrogen absorbing alloys. J Alloys Compd 2009;484:190–5.
[52] Wang F, Li R, Ding C, Tang W, Wang Y, Xu S, Wu Y. Recent progress on the hydrogen storage properties of Zr Co-based alloys applied in international thermonuclear experimental reactor (ITER). Prog Nat Sci: Mater Inter 2017;27:58–65.
[53] Anbarasu S. Studies on metal hydride based hydrogen storage device. PhD Thesis. IIT Guwahati; 2014.
[54] Evangelos MK, Gkanas I. Study on the hydrogenation of an Mm-based AB5-intermetallic for sustainable building applications. Int J Energy Res 2012. https://doi.org/10.1002/er.4794.
[55] Kumar Sharma Vinod, Anil Kumar E. Thermodynamic analysis of novel multi stage multi effect metal hydride based thermodynamic system for simultaneous cooling heat pumping and heat transformation. Int J Hydrogen Energy 2017;42:437–47.
[56] Mohan Man, Kumar Sharma Vinod. Perforamce investigation of novel multi stage multi effect sorption thermdynamic system for heating and cooling applications. Appl Therm Eng 2019;161:114097.
[57] Kumar Sharma Vinod, Anil Kumar E. Effect of measurement parameters on hydrogen storage and thermodynamic properties of La – based metal hydrides. Int J Hydrogen Energy 2014;39:5888–98.
[58] Stamatakis Emmanuel, Zoulias Emmanuel, Tzamalis George, Massina Zoe, Analytis Vassilis, Christodoulou Christodoulos, Stubos Athanasios. Metal hydride hydrogen compressors: current developments and early markets. Renew Energy 2018. https://doi.org/10.1016/j.renene.2018.04.073.

Nomenclature

ΔH: Absorption/Desorption enthalpy, kJ mol^{-1}
ΔS: Absorption/Desorption entropy, kJ mol^{-1} K^{-1}
φ, φ_0: PCI slope factors
ρ: Density, kg m^{-3}
β: PCI Hysteresis factor
λ: Thermal conductivity, W m^{-1} K^{-1}
C_a: Absorption rate constant, s^{-1}
C_d: Desorption rate constant, s^{-1}
E: Absorption/Desorption activation energy, kJmol^{-1} of H_2
$\dot{m}$: Mass flow, kg m^{-3} s
M: Molecular weight, kg $kmol^{-1}$
n: Moles of gas, mol
P_{eq}: Equilibrium pressure, bar
R_u: Universal gas constant, kJ mol^{-1} K^{-1}
T: Absolute temperature, °C
u: Velocity, m s^{-1}
wt%: Hydrogen concentration, %
x: Hydrogen concentration, (H/M ratio)

Subscripts

a: absorption
d: desorption